

Femtosecond Two-Photon Response Dynamics of Photomultiplier Tubes

Toshiaki HATTORI*, Yoshitsugu KAWASHIMA, Masahiro DAIKOKU, Hideyuki INOUE and Hiroki NAKATSUKA
Institute of Applied Physics, University of Tsukuba, Tsukuba 305-8573, Japan

(Received April 3, 2000; accepted for publication May 12, 2000)

An intermediate state of two-photon photoemission processes in a photomultiplier tube was found and relaxation with a time constant of 270 fs was observed by time-correlated measurements using 15 fs, 800 nm optical pulses. Optical Bloch equation analysis of the signal intensity was carried out using a perturbation method.

KEYWORDS: femtosecond, two-photon process, photomultiplier tube, photoemission, autocorrelation

1. Introduction

Recently, the two-photon-induced responses of photodetectors are attracting much attention because of their application in pulse-width measurements of ultrashort optical pulses.^{1–6} Two-photon-induced photocurrent in photodiodes (PDs),^{1–3} light-emitting diodes (LEDs),⁴ and photomultiplier tubes (PMTs)^{5,6} has been used for intensity autocorrelation measurements of picosecond or femtosecond optical pulses. This technique has greatly simplified the autocorrelation measurements, which were conventionally carried out using a second-harmonic-generation crystal, a wavelength-selective optical filter, and a sensitive photodetector. PMTs have been shown to be particularly useful for pulse-width measurement of weak pulses because of their very high sensitivity.⁷

In the case of using photodetectors in pulse-width measurements of ultrashort optical pulses, it is important to study the temporal behavior of the two-photon response of these detectors. Autocorrelation measurement of 6 fs pulses using a GaAsP PD has been reported² where no discernible broadening of the signal trace was observed. In PDs and LEDs, group-velocity dispersion of light in semiconductor materials is the major cause of limitation of time resolution.

In PMTs, on the other hand, the two-photon-induced photoemission can occur via a two-step process. Electrons in photocathode materials of PMTs can be excited to the conduction band when they attain energy greater than the bandgap energy. Photoemission, however, can occur only when the electrons attain energy greater than the sum of the bandgap energy and the electron affinity. In many photocathode materials of PMTs, the bottom of the conduction band is located well below the vacuum level.⁸ Thus, the two-photon process can have an intermediate state, which lies in the conduction band, and the photoemission can occur only after an electron is excited above the vacuum level from the conduction band by a second incident photon. In this case, the lifetime of the intermediate state determines the time resolution of the autocorrelation measurement. Therefore, it is very important to study the existence of an intermediate state in the two-photon photoemission process and to determine its lifetime, if it exists, for the application of photodetectors in the ultrashort pulse-width measurement.

In this paper, we report the time-resolved study of two-photon photoemission in PMTs, and our findings on the existence of an intermediate state of the two-photon photoemission process. We also discuss the experimental results ob-

tained by a perturbation method in the optical Bloch equation analysis. We propose a model for the photocathode material in a three-level system, and clarify the influence of the intermediate state lifetime and dephasing times on the two-photon photoemission signal trace.

2. Experiments and Results

The experimental setup is shown in Fig. 1. The light source was a home-built Kerr-lens mode-locked Ti:sapphire laser,^{7,9} which generates 15 fs pulses at 800 nm at a repetition rate of 89 MHz. The output average power of the laser was about 600 mW. The light power used in the experiment was controlled using a reflective variable attenuator. The attenuated light was transmitted to a Michelson-type interferometer. The output of the interferometer was loosely focused using a concave mirror with a focal length of 200 mm onto the photocathode of the PMT. The spot size of the incident beam on the detector was about 80 μm , which was measured by a knife-edge method. The average power of the light incident on the detector was measured using a power meter with a delay time of the interferometer larger than 300 fs, which ensured negligible interference between light from the two arms of the interferometer. Time-correlated signal traces were obtained by scanning the delay time of one arm of the interferometer using a translation stage driven by a microstep stepping motor.

Two types of PMTs were used in the experiment. One was a side-on-type PMT with a reflection-mode photocathode (1P28, Hamamatsu Photonics). The photocathode material of CS_3Sb . The other was a head-on-type PMT with a transmission-mode photocathode (R2557, Hamamatsu Photonics). The photocathode material is Na_2KSb . These PMTs have single-photon response spectra similar to that of

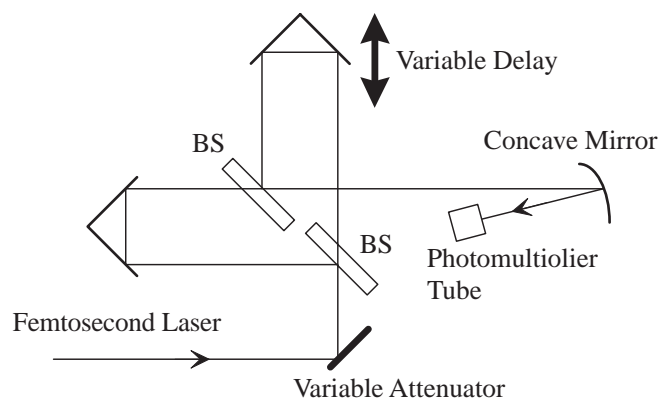


Fig. 1. Schematic of the experimental setup. BS: beamsplitter.

*E-mail address: hattori@bk.tsukuba.ac.jp

a GaAsP PD, which was used in the autocorrelation measurement of 6 fs pulses.²⁾ They have high sensitivity at 400 nm, and are almost insensitive to 800 nm light.

The delay-time dependence of the photocurrent obtained with a 1P28 PMT is shown in Fig. 2. The signal intensity is normalized at the baseline level. This trace has previously been reported elsewhere,⁷⁾ and is shown here only for comparison. The incident average power was $410 \mu\text{W}$. This trace agrees very well with the autocorrelation trace obtained with a GaAsP PD at incident light level of 10–100 mW, and well simulated with a 15 fs Gaussian pulse. This shows that the two-photon-induced process in this type of PMT can be regarded as essentially instantaneous in this time regime.

The signal trace obtained with an R2557 PMT is shown in Fig. 3. The average power of the incident light was $350 \mu\text{W}$. Note that data with a much larger range of delay times are shown here, compared with those in Fig. 2. The trace shows tails beside the oscillatory central part. The central part is similar to that of the trace obtained with a 1P28 PMT, as shown in Fig. 2. Tails similar to those in Fig. 3 are often seen in autocorrelation traces of significantly chirped pulses. However, in the present experiment, autocorrelation measurements of the same pulses with a GaAsP PD proved that the pulses were almost Fourier-transform limited. Pulse broadening of

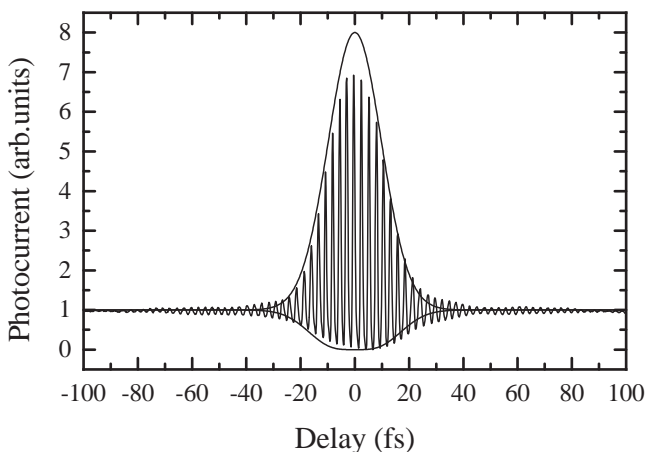


Fig. 2. Delay-time dependence of time-correlated photocurrent obtained using a 1P28 PMT. It is normalized at the baseline level. Envelopes of simulated autocorrelation trace of 15-fs Gaussian pulses are also shown.

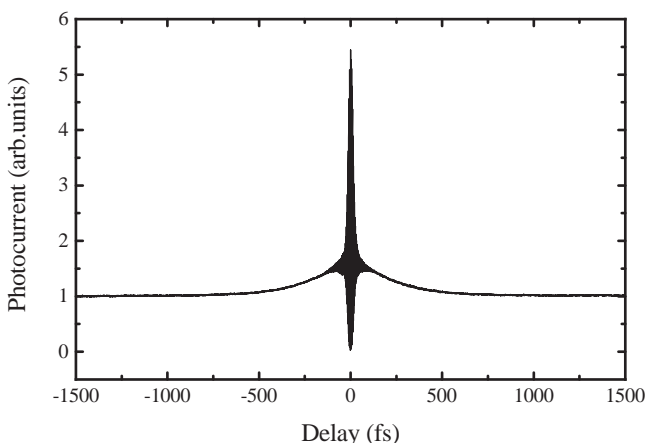


Fig. 3. Delay-time dependence of the time-correlated photocurrent obtained using an R2557 PMT. It is normalized at the baseline level.

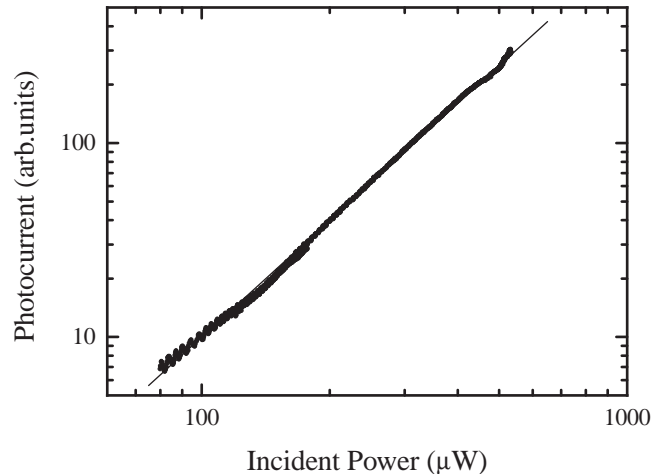


Fig. 4. Input power dependence of photocurrent of an R2557 PMT. Small circles indicate experimentally obtained data, and the straight line shows the best fit with line with a slope of 2.

a 15 fs pulse due to transmission through the 0.5-mm-thick window glass of the PMT is estimated to be only 0.6 fs. The existence of tails in the delay-time dependence of the two-photon-induced photocurrent in the PMT, therefore, should be attributed to a relaxation process in an intermediate state of the two-photon excitation process. The tails were well fitted with a single exponential function and the decay time was found to be 270 fs.

It has been reported that the bandgap energies of Cs_3Sb and Na_2KSb are 1.6 eV and 1.0 eV, respectively, although both of these materials have a similar value of the sum of the bandgap energy and the electron affinity at 2.0 eV.⁸⁾ These findings explain the observed results. Since the incident 800-nm light has a photon energy of 1.55 eV, it can induce interband transition with one photon in Na_2KSb , and electrons reach the vacuum level by two-photon absorption via a two-step process. In Cs_3Sb , on the other hand, no one-photon transition is possible with 1.55 eV incident light, and photoemission is induced by a direct two-photon process.

The incident power dependence of photocurrent obtained with an R2557 PMT is shown in Fig. 4. It is almost quadratic through the measured region of the power from 80 to $600 \mu\text{W}$. The dependence shows that two-photon-induced processes contribute dominantly to the photocurrent signal observed.

We will analyze the delay-time dependence of the two-photon photoemission signal obtained with an R2557 PMT by simulation using the optical Bloch equation.

3. Optical Bloch Equation Analysis

In the following, we derive the expression for the delay-time dependence of the two-photon-induced photoemission signal by solving the optical Bloch equation using a perturbation technique. A schematic for the energy levels of the model used here is shown in Fig. 5. We use a three-level model, where $|0\rangle$ is the ground level, $|1\rangle$ is the intermediate level of the two-photon transition, and $|2\rangle$ is the final level, from which photoelectrons are emitted. The energy differences between $|0\rangle$ and $|1\rangle$ and between $|1\rangle$ and $|2\rangle$ are assumed to be exactly resonant with the angular frequency, ω , of the incident light. Relaxation is taken into account by introducing phenomenological decay time constants, $T_1^{(1)}$ and $T_1^{(2)}$ for the

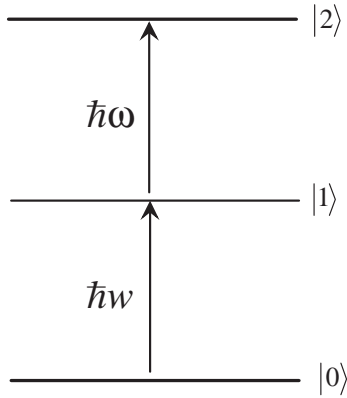


Fig. 5. Energy level scheme of the three-level model used in the theoretical treatment.

lifetimes of levels |1> and |2>, and $T_2^{(01)}$, $T_2^{(12)}$, and $T_2^{(02)}$ for the dephasing times between |0> and |1>, |1> and |2>, and |0> and |2>, respectively.

The Liouville equation of the density matrix of this system is expressed as

$$\frac{d}{dt}\rho(t) = \frac{i}{\hbar} [\mathcal{H}, \rho(t)] + \Gamma. \quad (1)$$

Here, $\rho(t)$ is the density matrix of the three-level system:

$$\rho(t) = \begin{bmatrix} \rho_{00}(t) & \rho_{01}(t) & \rho_{02}(t) \\ \rho_{10}(t) & \rho_{11}(t) & \rho_{12}(t) \\ \rho_{20}(t) & \rho_{21}(t) & \rho_{22}(t) \end{bmatrix}, \quad (2)$$

and the Hamiltonian of the system is

$$\mathcal{H} = \begin{bmatrix} 0 & 0 & 0 \\ 0 & \hbar\omega & 0 \\ 0 & 0 & 2\hbar\omega \end{bmatrix} - E(t) \begin{bmatrix} 0 & \mu_{01} & 0 \\ \mu_{01} & 0 & \mu_{12} \\ 0 & \mu_{12} & 0 \end{bmatrix}, \quad (3)$$

where $E(t)$ is the electric field of the incident light, and μ_{01} and μ_{12} are the transition dipole moments between |0> and |1> and between |1> and |2>, respectively, which are assumed to be real. The phenomenological relaxation term Γ in eq. (1) is expressed using the relaxation time constants as follows:

$$\Gamma = \begin{bmatrix} \rho_{11}(t)/T_1^{(1)} + \rho_{22}(t)/T_1^{(2)} & -\rho_{01}(t)/T_2^{(01)} & -\rho_{02}(t)/T_2^{(02)} \\ -\rho_{10}(t)/T_2^{(01)} & -\rho_{11}(t)/T_1^{(1)} & -\rho_{12}(t)/T_2^{(12)} \\ -\rho_{20}(t)/T_2^{(02)} & -\rho_{21}(t)/T_2^{(12)} & -\rho_{22}(t)/T_1^{(2)} \end{bmatrix}. \quad (4)$$

This type of optical Bloch equation has been used for the analysis of time-resolved two-photon photoemission signals of metals^{10–12} and superconductors.^{13,14} Results of numerical integration of the optical Bloch equation have been used for the study of T_1 and T_2 dependence of the signal trace, and simulation of experimentally obtained data.

In the present study, we apply a perturbation method to obtain analytical expressions of delay-time dependence of two-photon photoemission signals. By doing so, better physical insight can be obtained than by using numerical approaches. In the perturbation method, each element of the density matrix is expanded as:

$$\rho_{ij}(t) = \sum_{k=0}^{\infty} \rho_{ij}^{(k)}(t). \quad (5)$$

Here, $\rho_{ij}^{(k)}(t)$ is the term proportional to the k -th order of $E(t)$. It is assumed that the system is in the ground level when no light field is applied. That is,

$$\rho_{00}^{(0)}(t) = 1, \quad (6)$$

and all the other zero-th order elements vanish. By solving eq. (1) using the perturbation method, terms contributing to the signal intensity are derived as follows:

$$\rho_{01}^{(1)}(t) = \frac{i\mu_{01}}{\hbar} \int_{-\infty}^t E(t') \exp\left[-\left(i\omega + \frac{1}{T_2^{(01)}}\right)(t-t')\right] dt', \quad (7)$$

$$\rho_{02}^{(2)}(t) = \frac{i\mu_{12}}{\hbar} \int_{-\infty}^t E(t') \rho_{01}^{(1)}(t') \exp\left[-\left(2i\omega + \frac{1}{T_2^{(02)}}\right)(t-t')\right] dt', \quad (8)$$

$$\rho_{11}^{(2)}(t) = \frac{2\mu_{01}}{\hbar} \int_{-\infty}^t E(t') \Im[\rho_{01}^{(1)}(t')] \exp[-(t-t')/T_1^{(1)}] dt', \quad (9)$$

$$\rho_{12}^{(3)}(t) = \frac{i}{\hbar} \int_{-\infty}^t E(t') \left\{ \mu_{12} \rho_{11}^{(2)}(t') - \mu_{01} \rho_{02}^{(2)}(t') \right\} \exp\left[-\left(i\omega + \frac{1}{T_2^{(12)}}\right)(t-t')\right] dt', \quad (10)$$

$$\rho_{22}^{(4)}(t) = \frac{2\mu_{12}}{\hbar} \int_{-\infty}^t E(t') \Im[\rho_{12}^{(3)}(t')] \exp[-(t-t')/T_1^{(2)}] dt'. \quad (11)$$

Since $\rho_{22}(t)$ is the population of level |2>, the signal intensity is proportional to

$$I(\tau) = \int_{-\infty}^{\infty} \rho_{22}^{(4)}(t) dt. \quad (12)$$

Here, τ is the delay time of the second pulse with respect to the first pulse. By combining eqs. (11) and (12), we obtain

$$I(\tau) = \frac{2\mu_{12}T_1^{(2)}}{\hbar} \int_{-\infty}^{\infty} E(t) \Im[\rho_{12}^{(3)}(t)] dt. \quad (13)$$

This shows that the lifetime of level $|2\rangle$, $T_1^{(2)}$, has no effect on the shape of the delay time dependence of the signal intensity.

First, we study the case where $T_1^{(1)}$ is finite and dephasing times are much shorter than the pulse width. In this case, the signal intensity becomes proportional to a much simpler expression,

$$I(\tau) \propto I_1(\tau) = \int_{-\infty}^{\infty} dt \int_{-\infty}^t dt' E(t)^2 E(t')^2 \times \exp\left[-(t-t')/T_1^{(1)}\right]. \quad (14)$$

This expression can also be derived using a simple rate equation.

The incident electric field is assumed to consist of a pulse and a time-delayed replica of it:

$$E(t) = E_0(t) + E_0(t-\tau). \quad (15)$$

We assume the pulse shape here to be Gaussian:

$$E_0(t) = \frac{1}{2} \mathcal{E} e^{-t^2/\delta t^2} e^{-i\omega t - i\phi} + \text{c.c.} \quad (16)$$

Here, \mathcal{E} is the real amplitude, ϕ is the phase, and $\sqrt{2 \ln 2} \delta t$ is the width of the input pulse. Since the absolute phase of laser pulses cannot usually be controlled in actual experimental conditions, the experimentally obtained signal intensity should be the average over ϕ as

$$\begin{aligned} I_2(\tau) &= \langle I_1(\tau) \rangle_{\phi} \\ &= 4 \int_{-\infty}^{\infty} dt \int_{-\infty}^t dt' \exp\left[-(t-t')/T_1^{(1)}\right] |\tilde{E}(t)|^2 |\tilde{E}(t')|^2 \\ &\quad + \int_{-\infty}^{\infty} dt \int_{-\infty}^t dt' \exp\left[-(t-t')/T_1^{(1)}\right] \left\{ \tilde{E}(t)^2 \tilde{E}^*(t')^2 + \tilde{E}^*(t)^2 \tilde{E}(t')^2 \right\}. \end{aligned} \quad (17)$$

Here, $\langle \rangle_{\phi}$ means the average over ϕ , and $\tilde{E}(t)$ is defined as

$$\tilde{E}(t) = \frac{\mathcal{E}}{2} \left\{ e^{-t^2/\delta t^2 - i\omega t} + e^{-(t-\tau)^2/\delta t^2 - i\omega(t-\tau)} \right\}. \quad (18)$$

Although the effect of this averaging on the signal intensity is negligible when the pulse width is longer than a few periods of the oscillations of the optical field, it further simplifies the analytical expression. The contribution of the second term in eq. (17) to the signal intensity is negligible when

$$\omega^{-1} \ll \delta t, T_1^{(1)}. \quad (19)$$

Omission of this term corresponds to the rotating wave approximation. By omitting this term, the analytical expression for the signal intensity under these conditions is obtained as

$$\begin{aligned} I_2(\tau) &= \frac{\pi \delta t^2 \mathcal{E}^4}{8} \exp\left(\frac{\delta t^2}{4T_1^2}\right) \left\{ \operatorname{erfc}\left(\frac{\delta t}{2T_1}\right) \left(1 + e^{-\tau^2/\delta t^2}\right) \right. \\ &\quad + \frac{1}{2} \left[\operatorname{erfc}\left(\frac{\delta t}{2T_1} - \frac{\tau}{\delta t}\right) e^{-\tau/T_1} + \operatorname{erfc}\left(\frac{\delta t}{2T_1} + \frac{\tau}{\delta t}\right) e^{\tau/T_1} \right] \\ &\quad + 2 \left[\operatorname{erfc}\left(\frac{\delta t}{2T_1} - \frac{\tau}{2\delta t}\right) e^{-\tau/2T_1} + \operatorname{erfc}\left(\frac{\delta t}{2T_1} + \frac{\tau}{2\delta t}\right) e^{\tau/2T_1} \right] \cos(\omega\tau) e^{-\tau^2/2\delta t^2} \\ &\quad \left. + \operatorname{erfc}\left(\frac{\delta t}{2T_1}\right) \cos(2\omega\tau) e^{-\tau^2/\delta t^2} \right\}. \end{aligned} \quad (20)$$

Here, T_1 represents $T_1^{(1)}$, and $\operatorname{erfc}(x)$ is the complementary error function defined by

$$\operatorname{erfc}(x) = \frac{2}{\sqrt{\pi}} \int_x^{\infty} e^{-t^2} dt. \quad (21)$$

When T_1 is much longer than the pulse width;

$$T_1 \gg \delta t, \quad (22)$$

eq. (20) can be approximated by a much simpler form as follows:

$$\begin{aligned} I_2(\tau) &\propto 1 + e^{-\tau^2/\delta t^2} \\ &\quad + \frac{1}{2} \operatorname{erfc}\left(-\frac{\tau}{\delta t}\right) e^{-\tau/T_1} + \frac{1}{2} \operatorname{erfc}\left(\frac{\tau}{\delta t}\right) e^{\tau/T_1} \\ &\quad + 2 \left[\operatorname{erfc}\left(-\frac{\tau}{2\delta t}\right) e^{-\tau/2T_1} + \operatorname{erfc}\left(\frac{\tau}{2\delta t}\right) e^{\tau/2T_1} \right] \\ &\quad \times \cos(\omega\tau) e^{-\tau^2/2\delta t^2} \\ &\quad + \cos(2\omega\tau) e^{-\tau^2/\delta t^2}. \end{aligned} \quad (23)$$

The first term in eq. (23) gives the constant baseline value; second term, the nonoscillatory intensity autocorrelation function. The third and the fourth terms represent the tails which decay exponentially at a time constant of T_1 . The next term is for the

oscillating component with an angular frequency of ω , and the last term is for oscillations with an angular frequency of 2ω . Equation (23) is normalized at the baseline value, has a peak value of 8, and a tail amplitude of unity.

When $T_1^{(1)}$ is much shorter than the pulse width, on the other hand, eq. (20) is reduced to the fringe-resolved autocorrelation of the incident pulses as

$$\lim_{T_1 \rightarrow 0} \frac{I_2(\tau)}{T_1} = \frac{\pi\delta t \mathcal{E}^4}{8} \left[1 + 2e^{-\tau^2/\delta t^2} + 4e^{-3\tau^2/4\delta t^2} \cos(\omega\tau) + e^{-\tau^2/\delta t^2} \cos(2\omega\tau) \right]. \quad (24)$$

Simulation of signal traces was performed using eqs. (7)–(14). Pulse shape of the incident light was assumed to be Gaussian as in eq. (16), and the pulse width was fixed at 15 fs.

First, we assumed that the dephasing times, $T_2^{(01)}$, $T_2^{(12)}$, and $T_2^{(02)}$, are very short, and used eq. (14) for the simulation. Simulated delay-time dependence of the signal intensity with several values of the lifetime of the intermediate state, $T_1^{(1)}$, are shown in Fig. 6. The following features are seen in the plot. i) The signal has a peak value of 8 when it is normalized at the baseline level. ii) The tails have an amplitude of unity, and decay exponentially with a time constant of $T_1^{(1)}$. iii) The central oscillatory part is not deformed significantly by the existence of the intermediate state.

The trace with $T_1^{(1)} = 270$ fs agrees best with the experimentally obtained one, except that the peak-to-base ratio of the experimental trace is slightly lower. This suggests the existence of other intermediate states with decay times longer than the timescale of observation. It will raise the baseline level of the trace, and explains the disagreement of the experimental and the simulation traces.

Next, effects of finite dephasing times were studied. In the perturbation method, as shown in eq. (5)–(13), the fourth-order term, $\rho_{22}^{(4)}(t)$, which is responsible for the two-photon photoemission, is obtained via step-by-step integrations of lower-order terms through the paths shown in the following scheme:

$$\begin{array}{ccccccc} \rho_{00}^{(0)}(t) & \rightarrow & \rho_{01}^{(1)}(t) & \rightarrow & \rho_{02}^{(2)}(t) & & \\ & & \searrow & & \searrow & & \\ & & \rho_{10}^{(1)}(t) & \rightarrow & \rho_{11}^{(2)}(t) & \rightarrow & \rho_{12}^{(3)}(t) \\ & & & & \searrow & & \searrow \\ & & & & \rho_{20}^{(2)}(t) & \rightarrow & \rho_{21}^{(3)}(t) & \rightarrow & \rho_{22}^{(4)}(t). \end{array} \quad (25)$$

There are six different possible paths from $\rho_{00}^{(0)}(t)$ to $\rho_{22}^{(4)}(t)$. When conjugate elements are regarded as identical, only two different paths are possible. One path goes through $\rho_{11}^{(2)}(t)$, and the other through $\rho_{02}^{(2)}(t)$ or $\rho_{20}^{(2)}(t)$.

When the intermediate state lifetime, $T_1^{(1)}$, is finite, the integration path through $\rho_{11}^{(2)}(t)$ should make the major contribution to the signal intensity since the dephasing time between $|0\rangle$ and $|2\rangle$, $T_2^{(02)}$, is generally much shorter than the intermediate state lifetime. Thus, we neglect here the contribution of the integration through $\rho_{02}^{(2)}(t)$ and $\rho_{20}^{(2)}(t)$. The signal intensity obtained by the integration path through $\rho_{11}^{(2)}(t)$ is affected by two dephasing times, $T_2^{(01)}$ and $T_2^{(12)}$. These two

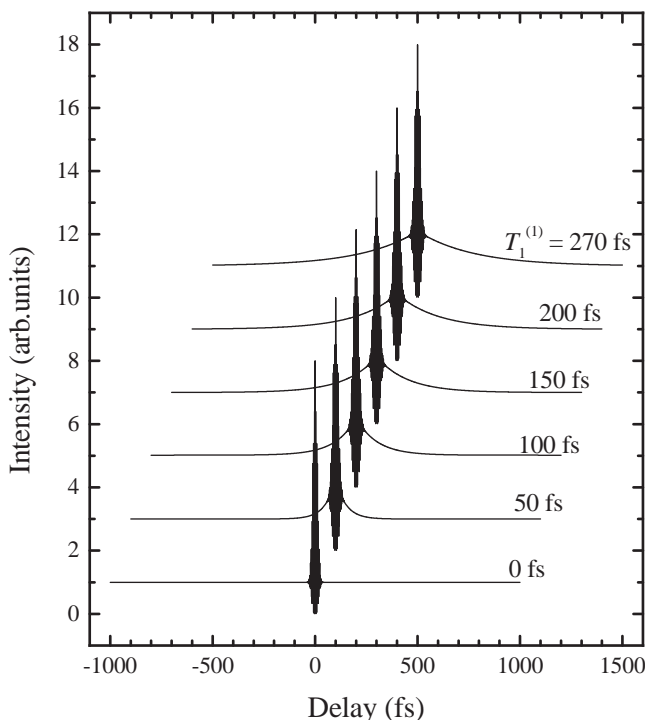


Fig. 6. Delay-time dependence of the signal intensity obtained by simulation with several values of lifetime of the intermediate state. Each trace is normalized at the baseline level, shifted rightward by 100 fs, and upward by 2.

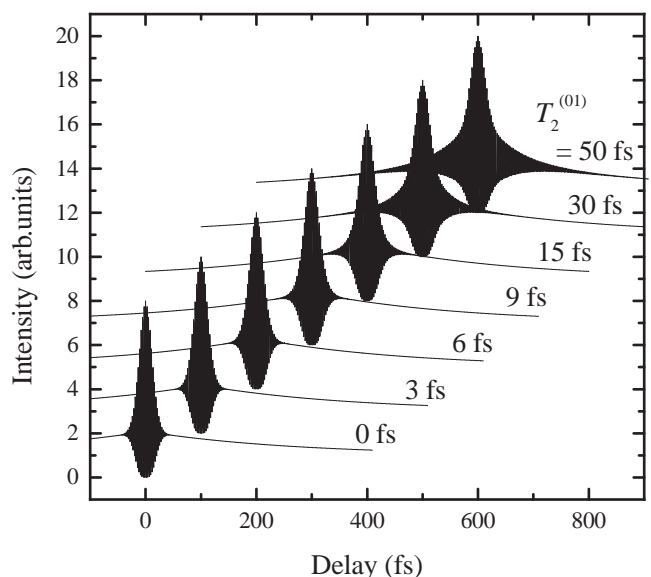


Fig. 7. Simulated signal traces with several values of the dephasing time between the ground and the intermediate state. The lifetime of the intermediate state is set at 270 fs. Each trace is normalized at the baseline level, shifted rightward by 100 fs, and upward by 2.

are expected to have similar effects on the signal shape, and here we simulated signal traces only with a finite $T_2^{(01)}$. The other dephasing times, $T_2^{(12)}$ and $T_2^{(02)}$ were set at zero. Traces calculated under these assumptions are shown in Fig. 7. The intermediate state lifetime was set at 270 fs, which is the experimental value. It is seen from the figure that when the dephasing time is finite, oscillations appear in the tails, and decay at a time constant of $T_2^{(01)}$. This agrees with the results of numerical calculations.¹⁰⁾ By comparing the simulated results with the experimentally obtained signal trace, the dephasing time of the photocathode material in the present PMT between the ground and the intermediate state is estimated to be equal to or less than 5 fs.

4. Conclusion

We measured the time-correlated photocurrent of two types of photomultiplier tubes. In one PMT, the signal was attributed to instantaneous two-photon photoemission, and the signal trace could be regarded as interferometric intensity autocorrelation of incident pulses. The signal trace of the other PMT had tails, which decay at a time constant of 270 fs. This was attributed to the existence of an intermediate state of the two-photon excitation process, which cannot be observed by linear optical measurements. Using a perturbation method in the optical Bloch equation analysis of the signal trace, analytical expressions for the signal trace were obtained. Signal traces were simulated using these theoretical results, and an intermediate state lifetime of 270 fs and dephasing time equal to or less than 5 fs were obtained from the experimental

data. The present results show that PMTs without one-photon response are not always suited for intensity autocorrelation measurements of ultrashort optical pulses using two-photon-induced processes in the photodetectors. This study also provides a new method to study dynamical properties of photoemissive materials and other photosensitive materials.

- 1) Y. Takagi, T. Kobayashi, K. Yoshihara and S. Imamura: *Opt. Lett.* **17** (1992) 658.
- 2) J. K. Ranka, A. L. Gaeta, A. Baltuska, M. S. Pshenichnikov and D. A. Wiersma: *Opt. Lett.* **22** (1997) 1344.
- 3) A. M. Streltsov, K. D. Moll, A. L. Gaeta, P. Kung, D. Walker and M. Razeghi: *Appl. Phys. Lett.* **75** (1999) 3778.
- 4) D. T. Reid, M. Padgett, C. McGowan, W. E. Sleat and W. Sibbett: *Opt. Lett.* **22** (1997) 233.
- 5) W. R. Bennett, Jr., D. B. Carlin and G. J. Collins: *IEEE J. Quantum Electron.* **10** (1974) 97.
- 6) Y. Takagi: *Appl. Opt.* **33** (1994) 6328.
- 7) T. Hattori, Y. Kawashima, M. Daikoku, H. Inouye and H. Nakatsuka: to be published in *Jpn. J. Appl. Phys.*
- 8) W. E. Spicer: *J. Appl. Phys.* **31** (1960) 2077.
- 9) T. Hattori, K. Kabuki, Y. Kawashima, M. Daikoku and H. Nakatsuka: *Jpn. J. Appl. Phys.* **38** (1999) 5898.
- 10) H. Petek and S. Ogawa: *Prog. Surf. Sci.* **56** (1997) 239.
- 11) S. Ogawa, H. Nagano, H. Petek and A. P. Heberle: *Phys. Rev. Lett.* **78** (1997) 1339.
- 12) H. Petek, A. P. Heberle, W. Nessler, H. Nagano, S. Kubota, S. Matsunami, N. Moriya and S. Ogawa: *Phys. Rev. Lett.* **79** (1997) 4649.
- 13) W. Nessler, S. Ogawa, H. Nagano, H. Petek, J. Shimoyama, Y. Nakayama and K. Kishio: *Phys. Rev. Lett.* **81** (1998) 4480.
- 14) W. Nessler, S. Ogawa, H. Nagano, H. Petek, J. Shimoyama, Y. Nakayama and K. Kishio: *J. Electron. Spectrosc. Relat. Phenom.* **88-91** (1998) 495.